Syntheses of Silver Nanoparticles in the Matrices of Block and Graft Copolymers and Polymer-Inorganic Hybrid in Aqueous Solutions

Sergey Fedorchuk,[*1] *Tatyana Zheltonozhskaya,*[1] *Yuriy Gomza,*[2] *Stanislav Nessin,*[2] *Larisa Kunitskaya,*[1] *Olga Demchenko*[1]

Summary: In the present work we have synthesized two-component block- and graft copolymers MOPEO-*b*-PAAm, PAAm-*b*-PEO-*b*-PAAm and PVA-*g*-PAAm comprised methoxypoly(ethylene oxide), poly(ethylene oxide) or poly(vinyl alcohol) and chemically complementary polyacrylamide and also the grafted polymer-inorganic hybrid SiO_2-*g*-PAAm based on monodispersed silica nanoparticles. These copolymers we used as special matrices in the process of borohydride reduction of Ag+ ions. It was established the influence of chemical nature, molecular architecture and concentration of the matrices and the content of silver nitrate on some reaction parameters, size and stability of Ag-nanoparticles in aqueous solutions.

Keywords: matrix; nanoparticles; self-assembly; small-angle X-ray scattering (SAXS); supramolecular structures

Introduction

The study of formation processes and physicochemical characteristics of metal nanoparticles creates the basis for their using in catalysis, optics, optoelectronics and other areas. In particular, silver nanoparticles are capable of forming complexes with drugs and delivering them in certain cells.[1] Due to antimicrobial activity, such nanoparticles are widely used as biocide agents in lacquers and paints, cosmetics, sewage filters and bandaging materials.[1–3] Polymer-metal nanocomposites with fractal aggregates of silver nanoparticles are prospective for creation of the optical recording systems and sensors.[4]

One of the actual aspects of modern nanotechnologies is development of the controlled methods of silver nanoparticle synthesis. The chemical reduction of silver ions has a great advantage among other methods due to high reproducibility of its results and possibility of generation a large amount of nanoparticles with narrow distribution in size. The type of reducing agent essentially influences on the nanoparticle formation. Stronger reducer stimulated the formation of less ''cores'' in ''embryos''.[5,6] During ''maturation'' process, which depended on foreign conditions, these ''cores'' were growing up to corresponding nanoparticles. Silver reduction is autocatalytic process, which consists in the adsorption of metal ions and their reduction on a surface of zero-valent particles.[7,8]

The second important aspect is stabilization of growing silver nanoparticles in solutions. At present, polymers are widely used for this purpose. Among stabilizers of silver nanoparticles there are homopolymers such as poly(ethylene glycol),[9] poly(vinyl pyrrolidon),[1] poly(pyridyl acetylene) etc.,[10] amphiphilic block copolymers,[11] graft copolymers,[12] and polymeric-inorganic hybrids.[13,14] Amphiphilic

[1] Department of Macromolecular Chemistry, Faculty of Chemistry, Kiev National Taras Shevchenko University, 64 Vladimirskaya St., 01033 Kiev, Ukraine Fax: +380442393100;
E-mail: sergey_fedorchuk@ukr.net
[2] Institute for Macromolecular Chemistry, National Academy of Sciences of Ukraine, 48 Kharkovskoye Shosse, 02160 Kiev, Ukraine

block and graft copolymers, which formed micellar structures, were used as stabilizers of silver nanodispersions mainly in organic mediums. But in many cases, especially at the application of Ag nanoparticles in medicine, biology, fragrance industry and catalysis of chemical reactions, they would be obtained and stabilized in aqueous medium.

The purpose of the present work was to study kinetic regularities and products of chemical (borohydride) reduction of Ag^+ ions from silver nitrate in aqueous solutions of polymer matrices with different chemical nature. We used as polymeric matrices: i) the block copolymers MOPEO-*b*-PAAm and PAAm-*b*-PEO-*b*-PAAm based on methoxypoly (ethylene oxide) or poly-(ethylene oxide) and polyacrilamide, ii) the graft copolymer PVA-*g*-PAAm contained poly(vinyl alcohol) and iii) the grafted polymer-inorganic hybrid SiO_2-*g*-PAAm comprised silica nanoparticles. The main peculiarity of said matrices consisted in the cooperative interaction of both their components that stipulated specific properties in aqueous solution. Indeed, the block and graft copolymers formed the intramolecular polycomplexes (IntraPCs) by means of hydrogen bonds between chemically complementary chains of MOPEO (PEO) and PAAm or PVA and PAAm.[15] This resulted in a self-assembly of the copolymer macromolecules into special micellar structures in dilute aqueous solutions. Also, due to existence of the hydrogen bond system between the grafted chains of PAAm and SiO_2 surface, the polymer-inorganic hybrid constituted the polymer-colloidal complex (PPC) in aqueous solutions.[16]

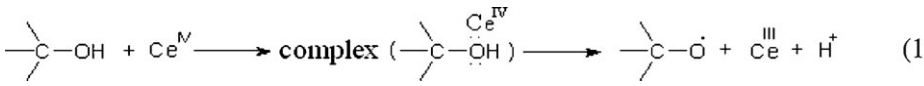

(1)

Synthesis and Characterization of Polymer Matrices

We carried out syntheses of MOPEO-*b*-PAAm diblock copolymer (DBC), PAAm-*b*-PEO-*b*-PAAm triblock copolymer (TBC) and PVA-*g*-PAAm graft copolymer and also the direct grafting PAAm chains onto SiO_2 surface using the template radical block and graft copolymerization, which was initiated by the Red/Ox reaction of cerium ammonium nitrate with hydroxyl groups of MOPEG, PEG and PVA (Scheme 1) or silanol groups of SiO_2 surface.[15–17]

We used in the syntheses the samples of MOPEG from ''Fluka'' (Germany), PEG and PVA from ''Aldrich'' (USA) with $M_v = 5$, 6 and 90 kDa, consequently, and also SiO_2 sol with the $R_g = 7.7$ nm particle size,[16] which was prepared from Aerosol A-175 (''Oriana'', Ukraine),. The molecular weights of PAAm blocks in DBC and TBC ($M_{nPAAm} = 29.8$ and 117.0 kDa, respectively) were determined by NMR spectroscopy.[18,19] More complicate characterization of PVA-*g*-PAAm and SiO_2-*g*-PAAm was described earlier.[15,16] The molecular weight and the average number of PAAm grafts in PVA-*g*-PAAm and SiO_2-*g*-PAAm were found to be $M_{vPAAm} = 147$ and 156 kDa, $N = 10$ and 23, consequently.

The state of DBC, TBC, PVA-*g*-PAAm and SiO_2-*g*-PAAm in aqueous solutions was considered in our previous publications.[15,16,18,20,21] It was shown that asymmetric macromolecules of DBC and TBC formed the ''hairy-type'' micelles in aqueous medium due to interaction of MOPEO (PEO) and PAAm blocks followed by segregation (self-assembly) of non-polar bound parts. Stability of DBC and TBC micelles, which was evaluated by both the critical micellization concentration and the Gibbs free micellization energy ($CMC = 1.3 \cdot 10^{-5}$ and $0.37 \cdot 10^{-5}$ mol $\cdot$ dm^{-3}; $-\Delta G^\circ = 32.98$ and 36.15, kJmol^{-1}, consequently), turned out to be higher for TBC. Relatively small ''core'' of these micelles contained non-polar bound parts of both the blocks but the developed ''corona''

comprised the segments of longer PAAm chains, which were unbound with PEO. Macromolecules of PVA-*g*-PAAm with chemically complementary components also formed the micelle-like associates,[15] which "corona" included the surplus PAAm segments unbound with PVA. Unlike this, "macromolecules" of SiO_2-*g*-PAAm formed a stable polymer-colloidal complex (PCC) in water because of adsorption of the grafts on SiO_2 surface.[21] Thus, free segments of PAAm stabilized the micelles of the block and graft copolymers and also the particles of PCC in water medium.

Kinetics and Products of Borohydride Reduction of Silver Ions

The reduction of silver ions was carried out in aqueous polymer solutions with the eightfold molar excess of $NaBH_4$ that allowed achieving practically complete conversion of Ag+ ions to zero-valent state in a selected region of $AgNO_3$ concentrations ($C_{AgNO3} = 0.91 \cdot 10^{-2}$ and $1.82 \cdot 10^{-2}\,kg \cdot m^{-3}$).[22] According to the studies,[23–25] the process of Ag+-ion reduction can be represented by the total stochiometric equation (2):

$$8Ag^{+} + BH_4^{-} + 8OH^{-} = 8Ag + H_2BO_3^{-} + 5H_2O \quad (2)$$

At the same time, borohydride anions participate also in some side reactions, due to which their essential excess is used to enhance the yield of Ag nanoparticles.[22–25]

Polymeric solutions was mixed with $AgNO_3$ and kept for 30 min in a dark box; then the reducing agent was added. We varied concentrations of the polymeric matrices ($C_m = 0.5$, 1.0 and $2.0\,kg \cdot m^{-3}$) and silver salt (see above). In 3–5 minutes after addition of the reducing agent to the mixtures of DBC, TBC, PVA-*g*-PAAm or SiO_2-*g*-PAAm with $AgNO_3$, a yellow coloring, which corresponded to the color of the diluted silver nanodispersions in water,[22,26] was appeared. The coloring intensity increased for 1–3 h at $C_{AgNO3} = 1.82 \cdot 10^{-2}\,kg \cdot m^{-3}$. But at lower concentrations of silver ions ($C_{AgNO3} = 0.91 \cdot 10^{-2}\,kg \cdot m^{-3}$) and at $C_m = 0.5$ and $1.0\,kg \cdot m^{-3}$, a yellow color was quickly disappeared and a black precipitate arose. The same picture was observed in the case of Ag+-ion reduction in polymer-free solutions with low concentration of $AgNO_3$.

The process of nanoparticle formation was controlled by the changes in the position (λ_{max}) and the integral intensity (S) of the surface plasmon resonance band (SPRB), which was displayed in a visible region of spectrum.[22,26] The time evolution of the extinction spectra was recorded in a three-minute interval in a region of 200–1000 nm using a Cary 50 Scan UV-Vis spectrometer from "Varian" (USA). The results for 90 min, which were obtained at the maximum concentrations of the matrices and $AgNO_3$, are shown in Figure 1.

In order to interpret these data, we used well-known optical properties of Ag nanoclusters/nanoparticles and theoretical approaches,[27–34] which allow connecting the position, intensity and shape of SPRB in the extinction spectra with the size, shape, polydispersity and aggregation of Ag nanoparticles in a solution. In particular, according to the Mie theory,[28] the total extinction coefficient of SPRB is determined by two contributions such as the resonant absorbance and scattering. But if the size of spherical Ag particles is <30 nm, the resonant absorbance introduces an overwhelming contribution to the extinction.[30] For said Ag particles, which size is much smaller than the wavelength of incident light, the absorbance A of a colloidal solution containing N particles in an optical cell with a path length L is: $A = (\kappa \cdot L)/\ln 10$, where the extinction coefficient κ for N particles of volume V is given by the (3) equation (the dipole term in the Mie formula):[29]

$$\hat{e} = \frac{18\pi \cdot N \cdot V \cdot \varepsilon_m^{3/2}}{\lambda} \frac{\varepsilon_2}{[\varepsilon_1 + 2 \cdot \varepsilon_m]^2 + \varepsilon_2^2} \quad (3)$$

Here λ is the wavelength of absorbing light, ε_m is the dielectric constant of

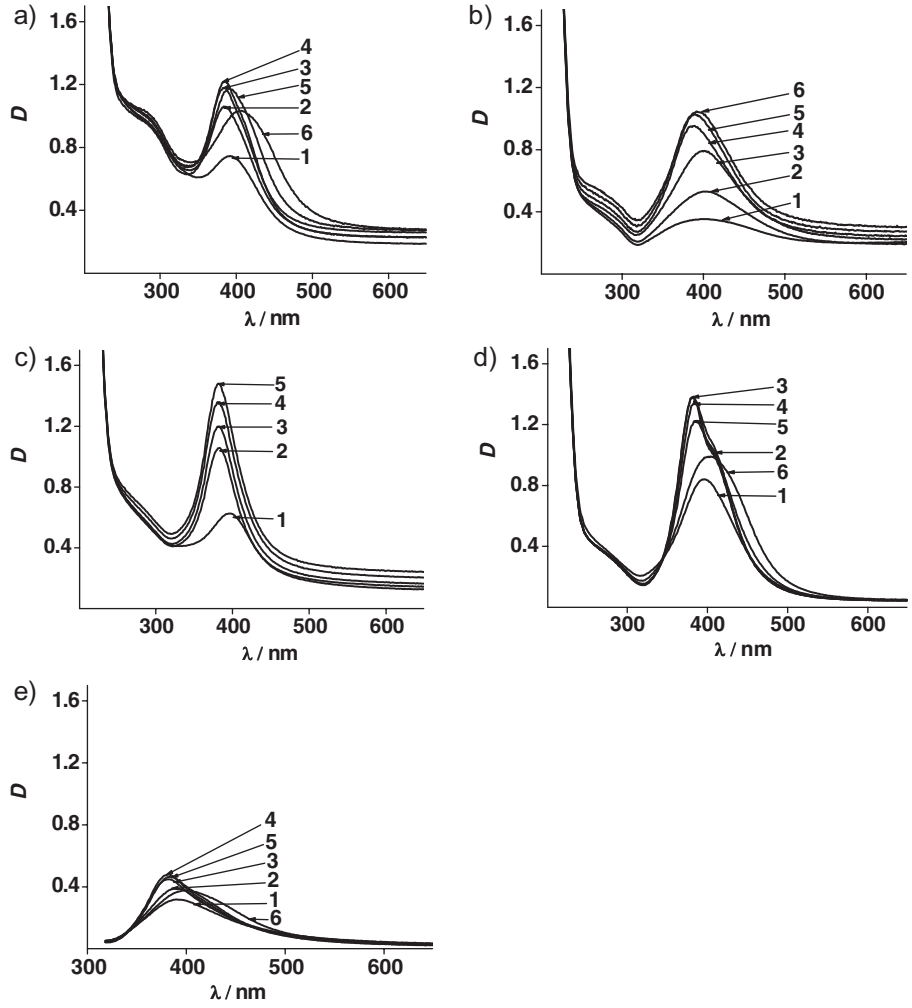

Figure 1.
The time evolution of the absorption spectra in aqueous blends of (**a**) MEPEO-*b*-PAAm, (**b**) PAAm-*b*-PEO-*b*-PAAm, (**c**) PVA-*g*-PAAm, (**d**) SiO_2-*g*-PAAm with $AgNO_3$ in 5 -1, 15 -2, 21 -3, 36 -4, 60–5 and 90 min –6 after $NaBH_4$ introduction.

surrounding medium (assumed to be frequency-independent), ε_1 and ε_2 are the real and imaginary parts of the material dielectric function $\varepsilon(\omega) = \varepsilon_1(\omega) + i \cdot \varepsilon_2(\omega)$, where ω is the angular frequency of the light. The width of SPRB mainly depends on the imaginary part of the dielectric function, which is responsible for dissipation of the electric field energy. But for silver unlike to other metals, $\varepsilon_2(\omega)$ value is insignificant and only weakly frequency-dependent.[31] Thus, in the pointed range of nano-sized Ag particles, the intensity of SPRB mainly depends on the particle concentration but not on the particle size.[27–29,31] Such property of SPRB is used (including the present work) to study kinetic regularities of the process of Ag nanoparticle formation in different conditions and time intervals, especially in the first minutes after beginning of the reduction reaction.

The formation of spherical Ag nanoparticles much smaller than the wavelength of light results in the appearance of a single

narrow SPRB with $\lambda_{max} = 380–425$ nm in the extinction spectra.[26,27,30,31,33] Exactly such Ag nanoparticles formed in the studied reaction blends that was confirmed by a unimodal narrow SPRB ($\lambda_{max} = 379–400$ nm), which was observed in all the spectra (Figure 1a-d). At the same time, in DBC and SiO_2-*g*-PAAm solutions and also in polymer-free solutions, such effects as SPRB widening in time and a red shift of λ_{max} were also revealed (Figure 1a, d, e). In principal, there are some reasons, which could initiate the last effects:[27–31,33,34] i) increase in a size (or polydispersity) of spherical Ag nanoparticles, ii) formation more stretched Ag particles (spheroids, ellipsoids etc.), and iii) aggregation of Ag nanoparticles. But taking into account the presence in the spectra (Figure 1a, d, e) only a single SPRB, we achieved the important conclusion about a small value of all proposed alterations in the above-mentioned systems. Indeed, in the case of a large increase in the Ag nanoparticle size, an additional (quadrupole) SPRB would appear in the spectrum. Analogous picture would observe, when strongly stretched Ag nanoparticles with a large aspect ratio or the developed aggregates of nanoparticles appear. It is seen, that Ag nanoparticles formed in PVA-*g*-PAAm solutions were the most stable in time (Figure 1c).

Note, that the Ag+-ion reduction was also occurred at the pointed C_{AgNO3} in polymer-free solutions (Figure 1e) but the yield of nanoparticles, which could be evaluated by the integral intensity S of SPRB (see discussion above), was less as compared to that in polymeric solutions. Similar results were obtained in the study[35] and explained by a small stabilizing action of Ag+ ions adsorbed on the surface of growing nanoparticles. But at lower C_{AgNO3}, the formation of stable enough Ag nanoparticles was not observed.

The spectra of all the reaction blends in Figure 1 demonstrated additionally a weak band in the region of $\lambda \sim 270–290$ nm. This absorption band is known to reflect the presence of the charged Ag_4^{2+} nanoclusters,[27] which arise at the initial stage of silver reduction. The maximum intensity of the band was observed in DBC solutions (Figure 1a).

Detail analysis of the results was carried out using the time dependences of the position (λ_{max}) and the integral intensity (S) of SPRB, which were derived from the data of Figure 1. The examples of such dependences for the process of Ag nanoparticle formation in PVA-*g*-PAAm and SiO_2-*g*-PAAm solutions are shown in Figures 2, 3.

Analysis of these kinetic curves showed some common phenomena and allowed determining the region of polymeric and $AgNO_3$ concentrations, in which the polymeric matrices controlled the process of Ag nanoparticle formation. Really, when the matrix influence was insignificant or absent, a steady increase in λ_{max} in time took place (as in two curves of Figure 2a and all curves of Figure 3a). Simultaneously, a small constant S value or its reduction in time (in any cases up to zero) was achieved due to decrease in the integral intensity or full disappearance of SPRB (Figures 2, 3c). In these cases the reduction reaction was developed too quickly and finished by the formation of the disordered aggregates of ''black'' silver. Significant influence of the polymeric matrices on the process of Ag nanoparticle formation consisted in a sharp increase in S value (Figure 2, 3d). Moreover, an interesting effect of simultaneous reduction in λ_{max} in 16–19 nm (Figure 2, 3b) was observed. One could be assumed that in these cases besides the increase in the yield of Ag nanoparticles due to their higher stabilization in a solution, the particle regulation (possibly crystallization) occurred. Invariable values of λ_{max} in a certain time region after their reduction pointed out the stability of nanoparticle parameters in this region.

In order to compare the activity of polymeric matrices in the reduction process, let's consider the kinetic parameters of the curves $S = f(t)$, which are represented in Table 1. A high rate of the nanoparticle accumulation (v_{max}) correlated as a rule with a small breakdown time (τ_0) and a high

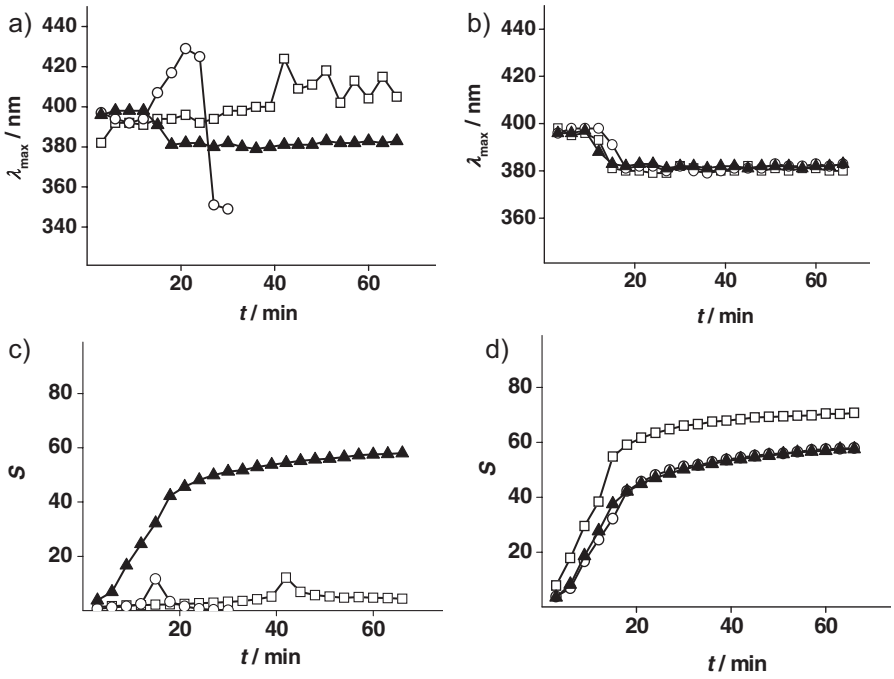

Figure 2.
Time dependences of (**a**, **b**) the position and (**c**, **d**) the integral intensity of SPRB in UV-Vis spectra, which were determined in PVA-g-PAAm aqueous solutions; $C_m = 0.5$ (□), 1.0 (○) and 2.0 kg · m^{-3} (▲), $C_{AgNO3} = 0.91 \cdot 10^{-2}$ (**a**, **c**) and $1.82 \cdot 10^{-2}$ kg · m^{-3} (**b**, **d**).

yield of Ag nanoparticles in a certain time (we selected 60 min) after reaction beginning (S_{60}). The parameter v_{max} corresponded to the slope of linear part of the curve $S = f(t)$, while the parameter τ_0 was determined by the intersection of this linear part with the abscissa axis. The building and state of the polymeric matrices played a key role in the reduction process. Actually, in spite of the same chemical nature of both the blocks in DBC and TBC macromolecules and a comparable length of PEO blocks in them, more stable TBC micelles (according to their thermodynamic parameters represented above) provided more quick increase in the amount of Ag nanoparticles even at small values of C_m and C_{AgNO3} (Table 1).

One could be assumed, that at the initial introduction of $AgNO_3$ into the block copolymer solutions, Ag+ ions interacted with amide groups of PAAm[36] and possibly with oxygen atoms of PEO, thus penetrating and concentrating not only in the ''corona'' of micelles but also in their ''core''. Then after addition of the reducer, the formation of Ag nanoparticles occurred under influence of the micelles. In this case, more stable micelles of TBC probably ensured a stronger protection from aggregation for the growing nanoparticles.

Some lesser values of v_{max} and S were fixed in PVA-*g*-PAAm solutions though exactly in this matrix at the large concentration of $AgNO_3$ silver nanoparticles demonstrated the highest stability (Figure 1c), which one remained during all time period unlike to the situation in DBC and SiO_2-*g*-PAAm solutions (Figure 1a, d).

The highest rate and nanoparticle yield for the first 60 minutes were observed in solutions of the polymer-inorganic hybrid (Table 1). The reason for this effect consisted to our opinion in a stronger

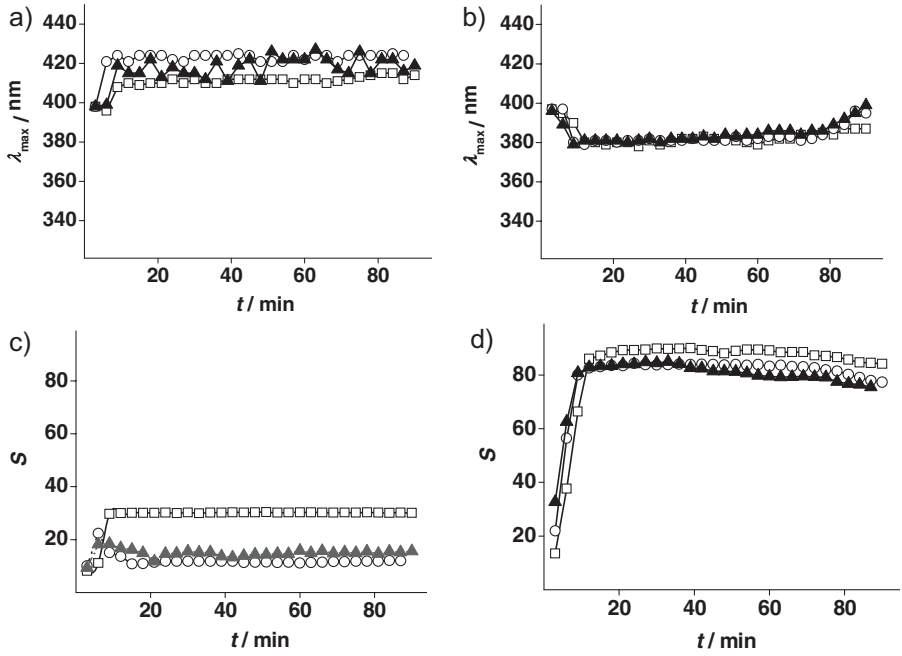

Figure 3.
Time dependences of (**a**, **b**) the position and (**c**, **d**) the integral intensity of SPRB in UV-Vis spectra recorded in SiO_2-*g*-PAAm aqueous solutions; $C_m = 0.5$ (□), 1.0 (○) and 2.0 $kg \cdot m^{-3}$ (▲), $C_{AgNO_3} = 0.91 \cdot 10^{-2}$ (**a**, **c**) and $1.82 \cdot 10^{-2}$ $kg \cdot m^{-3}$ (**b**, **d**).

interaction of Ag+ ions, nanoclusters and growing nanoparticles with the polymer-inorganic matrix as at the stage of $AgNO_3$ introduction in the system as in the reduction process. Indeed, on the one hand, pH values in SiO_2-*g*-PAAm solutions with $C_m = 0.5$, 1.0 and 2.0 $kg \cdot m^{-3}$ were found to be 5.2, 6.4 and 6.8, consequently. At these pH values, SiO_2 particles of the polymer-inorganic hybrid were negatively charged because the point of zero charge for SiO_2 sol particles in aqueous solutions was equal to pH = 3.0–3.5. On the other hand, Ag^+ ions are capable of connecting with negatively charged SiO_2 surface by strong electrostatic interactions unlike to their weaker complexation with oxygen atoms of PEO, hydroxyl groups of PVA and PAAm amide groups.[36] Therefore, in this case the reduction reaction will be proceeding mainly on SiO_2 surface, which will be a strong stabilizing factor also for the growing nanoparticles coated with Ag^+ ions.[37]

Long-Term Stabilization of Silver Nanoparticles

In order to compare stabilizing effect of the polymeric matrices over a longer time, UV-Vis spectroscopic studies of the reduction reactions in PVA-g-PAAm and SiO_2-g-PAAm solutions and also in pure water were performed for 10 days. In these researchers, the same matrix concentrations, the largest concentration of silver salt ($C_{AgNO3} = 1.82 \cdot 10^{-2}$ $kg \cdot m^{-3}$) and the eightfold excess of $NaBH_4$ relatively to silver salt were used. It should be noted that in all spectra only a single SPRB was observed. This band had symmetric character in the studied polymeric solutions but kept some asymmetry (as in Figure 1e) in the polymer-free solution. Based on these results, the dependences of λ_{max} and S versus time were constructed (Figure 4).

It is seen, that in PVA-*g*-PAAm solutions the accumulation of Ag nanoparticles

Table 1.
Kinetic parameters of the process of silver nanoparticle formation

Polymeric matrix	C_m	$C_{AgNO_3} \cdot 10^2$	τ_0 [a)]	$v_{max} \cdot 10^2$ [b)]	S_{60} [c)]
	$kg \cdot m^{-3}$	$kg \cdot m^{-3}$	min	s^{-1}	
–	–	1.82	11.8	7.4	43.7
DBC	0.5	0.91	8.3	1.6	1.3
		1.82	2.3	4.9	39.9
	1.0	0.91	11.4	2.2	3.5
		1.82	3.0	6.8	44.5
	2.0	0.91	7.7	1.5	3.6
		1.82	3.6	5.2	40.7
TBC	0.5	0.91	7.3	9.8	23.7
		1.82	9.5	18.9	75.5
	1.0	0.91	17.5	4.3	10.0
		1.82	5.1	9.3	80.6
	2.0	0.91	10. 8	18.0	46.8
		1.82	0	4,83	64.2
PVA-*g*-PAAm	0.5	0.91	36.8	3.9	4.7
		1.82	5.9	10.3	70.5
	1.0	0.91	10.8	5.2	0
		1.82	4.3	5.2	57.5
	2.0	0.91	3.9	5.0	57.6
		1.82	3.0	5.2	57.0
SiO_2-*g*-PAAm	0.5	0.91	4. 8	12.3	30.3
		1.82	1.7	13.9	89.2
	1.0	0.91	2.4	9.7	11.1
		1.82	2.6	32.7	83.2
	2.0	0.91	2.4	7.6	15.8
		1.82	1.7	24.5	79.5

[a)]The breakdown time.[b)]The rate of the fastest stage of the process.[c)]The silver nanoparticles yield in 60 min after the reduction beginning.

with practically fixed size (this was confirmed by practically unchanged λ_{max}) proceeded for 2 h. Then, their size sharply increased in a sufficiently narrow time interval ($\sim$ 1 h) that was reflected in such alterations of SPRB parameters: increase in λ_{max} in 30–33 nm (Figure 4a) and decrease in S value (Figure 4c). The last alteration could be explained by the change in the extinction coefficient of SPRB with growth of Ag particle size.[27–33] Some increase in λ_{max} and decrease in S value were continued up to $\sim$ 24 h and then both the parameters were practically unchanged up to 10 days, thus implying the completion of Ag nanoparticle formation in PVA-*g*-PAAm solutions. The lower PVA-*g*-PAAm concentration, the higher yield of stabilized Ag nanoparticles (the larger S in Figure 4c).

A similar picture was observed in SiO_2-*g*-PAAm solutions (Figure 4b, d) but the process of a considerable enlargement of the primary Ag particles began earlier (after $\sim$ 30 min); moreover, it was not so sharp as compared to PVA-*g*-PAAm solutions. The nanoparticle formation was finished after 24 h and further Ag nanoparticles were in fully stabilized state in the whole time region under study (up to 10 days). In SiO_2-*g*-PAAm solutions, we also observed higher yield of the stabilized nanoparticles (higher S value in Figure 4d) at the less matrix concentration; however, this effect was not so significant as in PVA-*g*-PAAm solutions.

A secondary growth of the Ag nanoparticle size (or possibly alteration in their shape) we observed also in the polymer-free solution in 50 min after reduction beginning (Figure 4) but the effect was essentially weaker. Moreover, the yield of nanoparticles was lower and the changes in their size (or shape) continued after 24 h.

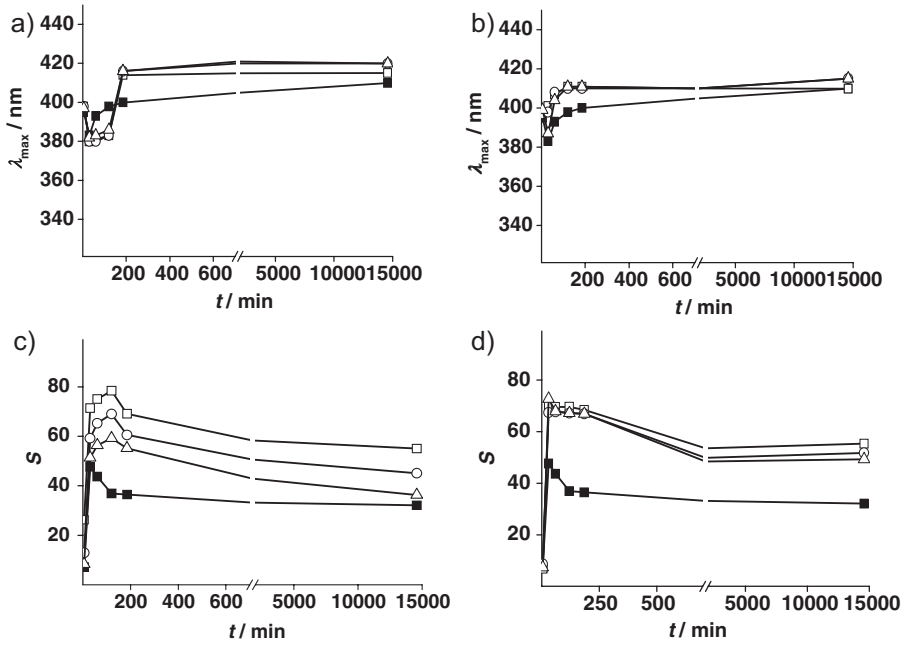

Figure 4.
Time dependences of (**a**, **c**) the integral intensity and (**b**, **d**) the position of SPRB in UV-Vis spectra, which were recorded in solutions of (**a**, **c**) PVA-*g*-PAAm, (**b**, **d**) SiO_2-*g*-PAAm and (**a–d**) in pure water; $C_m = 0$ (■), 0.5 (□), 1.0 (○) and 2.0 $kg \cdot m^{-3}$ (Δ), $C_{AgNO_3} = 1.82 \cdot 10^{-2}\, kg \cdot m^{-3}$.

Structure of Polymeric Compositions with Silver Nanoparticles

The bulk structure of some polymer-metal compositions was characterized and the size of Ag nanoparticles was determined using wide-angle and small-angle X-ray scattering (WAXS and SAXS). Two systems with PVA-*g*-PAAm and SiO_2-*g*-PAAm matrices, in which the high yield and time stability of silver nanoparticles were achieved (Table 1, Figure 4), were selected for this purpose. The polymer-metal compositions were cast from aqueous solutions ($C_m = 2.0$ and $C_{AgNO3} = 3.64\, kg \cdot m^{-3}$) into special Teflon forms placed in a dark box and then were dried on air and in a vacuum desiccator for 10 days.

WAXS profiles for the dried compositions were obtained in a cell with a thickness of 2 mm using a DRON-2.0 X-ray difractometer with Ni-filter in a primary beam. The monochromatic Cu-K_α radiation with $\lambda = 0.154$ nm, filtered by Ni, was provided by an IRIS M7 generator (at operating voltage of 30 kV and a current of 30 mA). The scattered intensities were measured by a scintillation detector scanning in 0.2° steps over the range of the $\theta = 3$–45° scattering angles (corresponding to $q = 2.13$–$31.21\ nm^{-1}$, where $q = 4\pi \cdot sin(\theta/2)/\lambda$ is the wavevector or the scattering vector). The diffraction curves obtained were reduced to equal intensities of the primary beam and equal values of the scattering volume.[38] Also, the normalization of experimental scattered intensities was carried out according to the (4) formula:

$$I_{n(i)}(\theta) = [I_{\exp}(\theta) - I_b(\theta)] \cdot (I/I_0); \qquad (4)$$

where $I_{exp}(\theta)$ and $I_{n(i)}(\theta)$ are the experimental and normalized intensities in WAXS profile as a function of θ, $I_b(\theta)$ is the intensity of the background for every θ value, I_0 and I are the intensities of incident and scattered beams at $\theta = 0°$ (the coefficient of the beam weakening). The results

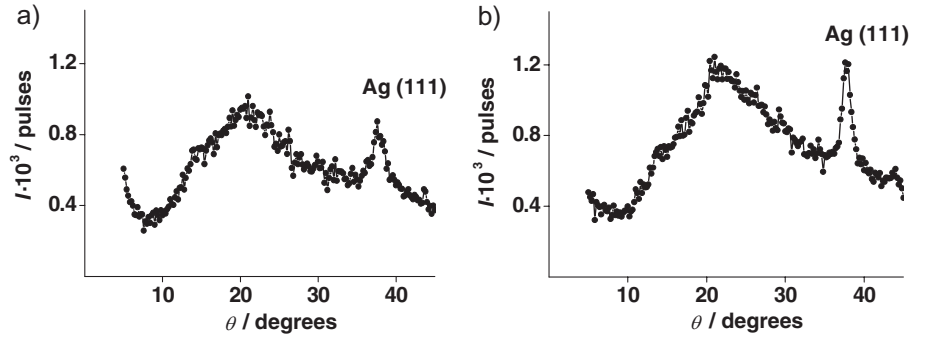

Figure 5.
WAXS difractograms for the compositions: (**a**) PVA-*g*-PAAm + Ag and (**b**) SiO_2-*g*-PAAm + Ag. $T = 20\ ^\circ C$.

(Figure 5) showed that the bulk structure of the compositions contained a polymeric amorphous phase, that was displayed in WAXS profiles by two diffusive overlapped maxima at $\theta \sim 15^\circ$ and 21°, and crystalline Ag nanoparticles, that was confirmed by characteristic crystalline peaks of silver (111) at $\theta \sim 38^\circ$.[6] The appearance of these peaks indicated the formation of crystalline Ag nanoparticles with tetragonal facet-centered cubic lattice.[6] An amorphous character of polymeric phases in the compositions was completely correlated with the data of DSC studies,[16,21,19,39] which demonstrated the loss of PVA crystalline properties in the graft copolymer structure because of the interaction of the main and grafted chains and also the existence of only glass transitions in PVA-*g*-PAAm and SiO_2-*g*-PAAm structures at their heating.

As to the presence of two diffusive overlapped maxima in WAXS profiles in Figure 5, they could be attributed (as in the study[39]) to the presence of two systems of planes of the paracrystalline lattice[38] in the amorphous regions of PVA-*g*-PAAm and SiO_2-*g*-PAAm structures, which contain mainly PAAm chains. The first maximum with smaller intensity at $\theta \sim 15^\circ$characterizes the lateral periodicity in an arrangement of PAAm chains but the second one with greater intensity at $\theta \sim 21^\circ$ reflects the periodic arrangement of the flat hydrogen-bonded *cis*-dimers of amide groups in the structures of *cis-trans*-multimers.[15] More exact positions of these maxima and the average interplane distances (d) in the paracrystalline lattice of amorphous polymeric phase and the crystalline lattice of silver nanoparticles (the last ones were calculated by the Bragg ratio (5)) are represented in Table 2.

$$d = \frac{\lambda}{2 \cdot \sin(\theta/2)}; \tag{5}$$

SAXS profiles for the compositions and SiO_2-*g*-PAAm sample were obtained in an automated Kratky slit-collimated camera. Here copper anode emission monochromated by total internal reflection and nickel filter was used. The intensity curves were recorded in the step-scanning mode of the

Table 2.
Parameters of diffraction maxima in WAXS profiles

Polymer matrix	Position of the diffraction maximum			The average interplane distance		
	θ_1	θ_2	θ_3	d_1	d_2	d_3
	degrees	degrees	degrees	nm	nm	nm
PVA-*g*-PAAm	~15.2	21.0	37.7	0.582	0.423	0.238
SiO_2-*g*-PAAm	~14.3	21.2	37.8	0.619	0.419	0.238

scintillation detector in a region of the $\theta = 0.03$–4.0° scattering angles (the wavevector $q = 0.022$–$2.86\,nm^{-1}$). Thus, the study of the micro-scale heterogeneous domains with characteristic dimensions (evaluated as $2\pi/q$) from 2 to 280 nm was possible. Normalization of SAXS profiles was carried out using the FFSAXS-3 program[38] and a standard sample from the laboratory of professor Kratky. The scattered intensities were normalized to the sample thickness and the scattered intensity of a standard. Additionally, the raw intensity curves were smoothed, corrected for parasitic scattering and desmeared. The results in a form of the dependences of the scattered intensities versus q are shown in Figure 6.

All the profiles demonstrated a sharp fall in the scattered intensities with q growth (without any diffraction maxima) that pointed out the absence of any periodicity in the arrangement of structural elements of the compositions and polymer-inorganic hybrid at the supramolecular level. The same profiles in two logarithmic coordinates are exhibited in Figure 6 in a lesser scale. Let's carry out their analysis from the point of view the fractal-cluster organization of the composition structure.[40]

The double logarithmic SAXS profiles for both the compositions and SiO_2-*g*-PAAm demonstrated two linear parts with different slopes, which corresponded to two power scattering regimes by Porod ($I \approx q^{-Df}$, where D_f is the slope ratio for corresponding straight line of log I *vs* log q). These linear parts were connected by the curve, which conformed to the exponential scattering regime by Guinier.[40] Such form of SAXS profiles in the double logarithmic coordinates pointed out the two-level fractal organization of a bulk structure of the compositions and polymer-inorganic hybrid. The character of separate elements of each level (the mass-fractal clusters, the surface-fractal clusters or solid particles with a smooth surface) could be determined by analysis of D_f value but the maximum diameter of these elements could be estimated by the relation $d_{max} \sim 2\pi/q^*$.[38,40] Finding the last parameter is possible in the case, when the straight line corresponding to the power scattering regime by Porod is ended (or ''cuts'') by the scattering regime by Guinier in the region of small q that is when a separate structural level is clearly displayed. A definite q^* value, which is determined in the region of the Guinier's scattering (Figure 6),[40] is considered as ''the cutting border''. All said parameters (D_f, q^* and d_{max}) were established only for the 1-st lower level of structural organization of the compositions and SiO_2-*g*-PAAm, which was displayed at higher q. For the 2-nd higher structural level, which was revealed at less q, only D_f numbers were found (Table 3) because corresponding straight lines of the Porod's scattering in

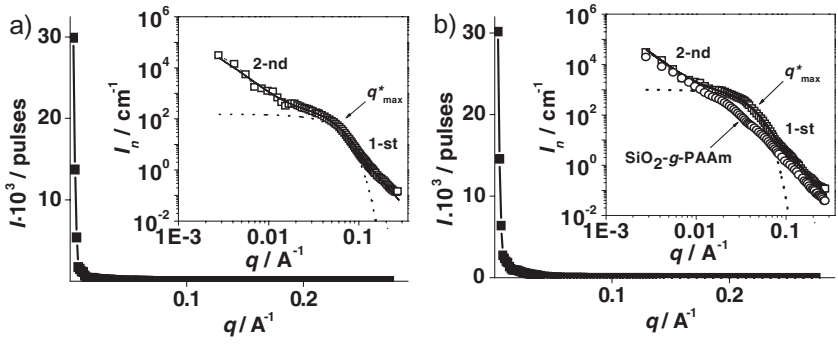

Figure 6.
The intensity of small-angle X-ray scattering *vs* the wavevector for the compositions: (**a**) PVA-*g*-PAAm + Ag and (**b**) SiO_2-*g*-PAAm + Ag. SAXS profile for a pure SiO_2-*g*-PAAm was analogous. The double logarithmic SAXS profiles are shown in a lesser scale; □ (**a**) = PVA-*g*-PAAm + Ag, □ (**b**) = SiO_2-*g*-PAAm + Ag, ○ (b) = SiO_2-*g*-PAAm.

Table 3.
Parameters of separate elements of the 1-st and 2-nd structural levels

System	PVA-*g*-PAAm +Ag		SiO_2-*g*-PAAm		SiO_2-*g*-PAAm +Ag	
Value	1-st	2-nd	1-st	2-nd	1-st	2-nd
D_f	4.0	2.6	3.8	2.1	4.0	2.5
$q^* \cdot 10^2/A^{-1}$	6.1	–	2.7	–	4.2	–
d_{max}/nm	10.3	–	23.3	–	15.0	–
R_g/nm	4.0	–	9.0	–	5.8	–
$R_{g\ (calc)}$/nm	3.5	–	8.0	–	5.5	–

Figure 6 were not restricted from above by the Guinier's scattering regimes.

It is well known,[40] that the $D_f = 4$ value characterizes the power scattering regime by Porod in the case of the dense solid scattering particles with a smooth surface. Exactly such values were determined for the linear parts of SAXS profiles, which corresponded to the 1-st structural level of the compositions (Table 3). This fact additionally confirmed the formation of the dense Ag nanoparticles in both the polymeric matrices. The maximum radius of a gyration for these particles was calculated using d_{max} value and the relation: $[R_g = d_{max}/2(5/3)^{1/2}]$.[40] It turns out to be essentially less in the composition with PVA-*g*-PAAm (Table 3). Thus, the dense crystalline Ag nanoparticles constituted the 1-st level of the fractal-organized structure of the polymer-metal composites.

A near value of $D_f = 3.8$ was found for an analogous linear part of SAXS profile of a pure SiO_2-g-PAAm (Table 3). This fact indicated the existence of the surface-fractal clusters with the fractal size $D_s = 6 – D_f = 2.2$,[40] which ones constituted the 1-st fractal-organized structural level of the polymer-inorganic hybrid. This result was the direct proof for the presence of SiO_2 nanoparticles with the grafted polymer chains in the hybrid structure. Note, that the radius of a gyration for these surface-fractal clusters (9.0 nm) that was found from SAXS data fully correlated with the $R_g = 7.7$ value, which was established for SiO_2 sol particles before PAAm grafting.

The mass-fractal clusters composed of the fragments of polymeric chains (mainly of PAAm segments) could be considered as separate elements of the 2-nd higher level in a structural organization of the polymer-metal composites and SiO_2-g-PAAm. Such conclusion was based on the $D_f < 3$ numbers, which were determined for this structural level from Figure 6 (Table 3).[40] The found numbers were fully coordinated with the values of $D_f = 2.7$ and $D_f = 2.2 \div 2.4$ characterized the mass-fractal clusters in the structure of pure PAAm and PAAm-*b*-PEO-*b*-PAAm triblock copolymers, consequently.[39]

The computer modeling of SAXS profiles by the method of global unified exponential-power functions, which was designed by Beaucage with co-workers,[41] is actively used in the studies of fractal-organized polymeric and composition materials.[40,41] These authors showed that the double logarithmic SAXS profiles for fractal-organized materials could contain two or more power regimes. Their approach consisted in the separation of several structural levels (in accordance with the number of the power scattering regimes), which were limited from above by the exponential scattering regimes by Guinier, and consideration of separate contributions from each structured level to the total scattering function. The equation (6) describes the arbitrary number of interrelated structural levels:[40,41]

$$I(q) = \sum_{i=1}^{n} (G_i \exp(-q^2 R_{g_i}^2/3) + B_i \exp(-q^2 R_{g_{(i+1)}}^2/3) \times \left\{ \left[erf(qR_{g_i}/6^{1/2}) \right]^3 / q \right\}^{P_i}) \quad (6)$$

Here G_i is the coefficient of Guinier's relation for *i*-level; B_i is the coefficient of

Porod's term for the same level; D_f is the slope ratio for the power dependence of log I versus log q, which one defines the fractal dimension of the aggregates by i-level (for the surface fractals $-4 < D_f < -3$ while for the mass fractals $D_f > -3$); R_g is the radius of a gyration for the fractal aggregates by i-level.

Using Beaucage's method, we modeled SAXS profiles for both the compositions and SiO_2-g-PAAm (solid curves in Figure 6) taking into consideration two levels of their structural organization, which were discussed above. The $R_{g(calc)}$ values, which were calculated by Beaucage's approach for: i) Ag nanoparticles in the composition structure and ii) the surface-fractal clusters with "cores" of SiO_2 particles in a bulk structure of the polymer-inorganic hybrid (Table 3), turned out to be in well agreement with those found from experimental SAXS profiles.

Conclusion

Thus, the block- and graft copolymers PAAm-*b*-PEO-*b*-PAAm and PVA-*g*-PAAm, which form IntraPCs and self-assemble in micellar structures in aqueous solutions, and also the grafted polymer-inorganic hybrid SiO_2-g-PAAm forming a stable PCC could be considered as efficient nanoreactors. They are capable of ensuring the high rate and efficacy of the borohydride reduction of silver ions up to the stable crystalline Ag nanoparticles with $R_g \sim$ 3-6 nm. Four stages of Ag nanoparticle formation in the presence of these polymeric matrices (in the region of polymer and $AgNO_3$ concentrations, where stabilizing effect was displayed) could be selected. At the first stage ($\sim$ 3–12 min), the appearance of Ag nanoclusters and unregulated Ag particles occurred. The nanoparticle regulation (possibly crystallization) developed in a very narrow time interval ($\sim$ 6 min) at the second stage, when the quantity of the unregulated Ag particles in the system became a large enough. This process resulted in the appearance of the primary regulated Ag nanoparticles. A state of these particles was not practically changed at the third stage, which duration was dependent on the nature and concentration of a polymeric matrix. At the end stage, an intense secondary growth of nanoparticle size or possibly alteration in their shape took place.

The compositions of PVA-*g*-PAAm and SiO_2-g-PAAm with Ag nanoparticles showed the two-level fractal organization of their structure. The dense crystalline silver nanoparticles were the separate elements of the 1-st lower level, while the mass-fractal clusters of the polymeric matrices constituted the 2-nd higher structural level.

[1] S. Kittler, C. Greulich, M. Köller, M. Epple, *Mat.-wiss. u. Werkstofftech.* **2009**, *40*, 258.
[2] G. Schmid, "*Nanoparticles: From theory to application.*", Weinheim Wiley-CH Verlag GmbH & Co, **2004**.
[3] O. Kalayc, F. Comert, B. Hazer, T. Atalay, K. Cavicchi, M. Cakmak, *Polym. Bull.* **2010**, *65*, 215.
[4] L. Sjulson, G. Miesenböck, *Physiology*. **2007**, *22*, 47.
[5] Yu. Plyuto, J.-M. Berquier, C. Jacquiod, C. Ricolleau, *Chem. Commun.* **1999**, 1653.
[6] E. A. Becturov, S. E. Kudaybergenov, A. K. Garmagambetova, R. M. Iskakov, J. E. Ibraeva, S. N. Shmakov, "*Polymer-protected metal nanoparticles*", Almaty **2010**, 274.
[7] P.-Y. Silvert, R. Herrera-Urbina, N. Duvauchelle, V. Vijayakrishnan, K. Tekaia-Elhsissen, *J. Mater. Chem.* **1996**, *6*, 573.
[8] P.-Y. Silvert, R. Herrera-Urbina, N. Duvauchelle, V. Vijayakrishnan, K. Tekaia-Elhsissen, *J. Mater. Chem.* **1997**, *7*, 293.
[9] A. Schadlich, C. Rose, J. Kuntsche, H. Caysa, T. Mueller, A. Gopferich, K. Mader, *Measurements Pharm. Res.* **2011**, *28*, 95.
[10] Yu. Mao, Hai Peng Xu, Hui Zhao, Wang Zhang Yuan, Anjun Qin, Yong Yu, Mahtab Faisal, *J. Mater. Chem.* **2011**, *21*, 13627.
[11] S. Förster, *Topics in Current Chemistry*. **2003**, *226*, 1.
[12] C. Rodriguez-Abreu, M. Lazzari, D. Varade, M. Kaneko, K. Aramaki, M. A. L. Quintela, *Colloid Polym. Sci.* **2007**, *285*, 673.
[13] L. Qiu, J. Franc, A. Rewari, D. Blancb, K. Saravanamuttu, *J. Mater. Chem.* **2009**, *19*, 373.
[14] S. De, G. De, *J. Mater. Chem.* **2006**, *16*, 3193.
[15] T. Zheltonozhskaya, N. Permyakova, L. Momot, in: "*Hydrogen-Bonded Interpolymer Complexes. Formation,*

Structure and Applications'', Ch.5, V. V., Khutoryanskiy, G. Staikos, New Jersey-London-Singapore-Beijing etc. World Scientific, **2009**.
[16] S. Filipchenko, O. Demchenko, T. Zheltonozhskaya, V. Syromyatnikov, *Radom University of Technology*. **2007**, 87.
[17] T. B. Zheltonozhskaya, S. V. Fedorchuk, V. G. Syromyatnikov, *Russ. Chem. Rev.* **2007**, *76*, 731.
[18] L. Kunitskaya, T. Zheltonozhskaya, S. Berkova, *The chemistry and chemical technology questions*. **2007**, *3*, 74.
[19] S. V. Fedorchuk, T. B. Zheltonozhskaya, E. M. Shembel, L. R. Kunitskaya, I. M. Maksuta, Y. P. Gomza, *Functional materials*. **2011**, *18*, 1.
[20] L. R. Kunitskaya, V. A. Aleinichenko, T. B. Zheltonozhskaya, S. A. Berkova, *Mat.-wiss. u. Werkstofftech*. **2010**, *42*, 109.
[21] O. Demchenko, T. Zheltonozhskaya, S. Filipchenko, V. Syromyatnikov, *Macromol. Symp*. **2005**, *222*, 103.
[22] B. Sergeev, L. Lopatina, A. Prusov, G. Sergeev, *Colloid. J.* **2005**, *67*, 79.
[23] N. N. Maltceva, V. S. Hain, ''*Sodium borohydride. Characteristic and application*'', Nauka, Moscow **1985**.
[24] H. C. Broun, A. C. Boyd, *Anal. Chem.* **1955**, *27*, 156.
[25] L. F. Holnstedt, B. O. Miniatas, *Anal. Chem*. **1965**, *37*, 1163.
[26] S. Horikoshi, H. Abe, K. Torigoe, M. Abe, Nick. Serpone, *Nanoscale*. **2010**, *2*, 1441.
[27] A. Henglein, *J. Phys. Chem*. **1993**, *97*, 5457.
[28] U. Kreibig, M. Vollmer, ''*Optical Properties of Metal Clusters*'', Springer, Berlin **1995**.
[29] S. Link, M. A. El-Sayed, *J. Phys. Chem. B*. **1999**, *103*, 8410.
[30] K. L. Kelly, E. Coronado, L. L. Zhao, G. C. Schatz, *J. Phys. Chem. B*. **2003**, *107*, 668.
[31] D. D. Evanoff, Jr., G. Chumanov, *Chem. Phys. Chem*. **2005**, *6*, 1221.
[32] L. M. Liz-Marzan, *Langmuir*. **2006**, *22*, 32.
[33] A. Yu, A. A. Krutyakov, A. Kudrinskiy, Yu. Olenin, G. V. Lisichkin, *Russ. Chem. Rev*. **2008**, *77*, 233.
[34] B. Sergeev, M. Kiruyhin, A. Prusov, G. Sergeev, [in Russian] *Moscow Univ. Bull*. **1999**, *40*, 129.
[35] D. G. Angelescu, M. Vasilescu, R. Somoghi, D. Donescu, V. S. Teodorescu, *Colloids and Surfaces A: Physicochem Eng. Asp*. **2010**, *366*, 155.
[36] V. Romanov, C.-K. Siu, U. H. Verkerk, H. El Aribi, A. C. Hopkinson, K. W. Michael Siu, *J. Phys. Chem. A*. **2008**, *112*, 10912.
[37] T. Kravchenko, N. Nikolaev, ''*Kinetics and dynamics of processes in RedOx ions*'', [in Russian] Chemistry, Moscow **1982**.
[38] Yu. S. Lipatov, V. V. Shilov, Yu. P. Gomza, et al. ''*X-Ray Diffraction Methods to Study Polymeric Systems*'', Nauk. Dumka, Kyiv **1982**.
[39] S. Fedorchuk, T. Zheltonozhskaya, N. Permyakova, Y. Gomza, S. Nessin, V. Klepko, *Mol. Cryst. Liq. Cryst*. **2008**, *497*, 268.
[40] A. P. Shpak, V. V. Shilov, O. A. Shilova, Yu. A. Kunitskiy, ''*Diagnostics of nanosystems. Multilevel fractal structures*'', Nauk. Dumka, Kyiv **2004**.
[41] G. Beaucage, J. Hyeonlee, Se. Pratsinis, S. Vemury, *Langmuir*. **1998**, *14*, 5751.

